Electron elastic scattering and low-frequency bremsstrahlung on $A@C_{60}$: A model static-exchange approximation

V. K. Dolmatov, C. Bayens, M. B. Cooper, and M. E. Hunter
Department of Physics and Earth Science, University of North Alabama, Florence, Alabama 35632, USA
(Received 25 February 2015; revised manuscript received 20 April 2015; published 4 June 2015)

Electron elastic-scattering phase shifts and cross sections as well as total cross sections of low-frequency bremsstrahlung and its angular-asymmetry and polarization parameters upon low-energy electron collision with endohedral fullerenes $A@C_{60}$ are theoretically scrutinized versus the nature, size, and spin of the encapsulated atom A. This is achieved by choosing Ar, Xe, Ba, Cr, Mn, and Eu as the case-study atoms A. The aim is to uncover the variety of effects which might occur in the above processes rather than to make thorough predictions for one particular spectrum. To that end, the study makes use of a simple model static-exchange approximation. There, both the encapsulated atom A and the C_{60} cage are regarded as nonpolarizable targets and the C_{60} cage itself is modeled by an attractive spherical annular potential well. Calculated results identify the most interesting and/or useful future measurements or more rigorous calculations to perform.

DOI: 10.1103/PhysRevA.91.062703 PACS number(s): 34.80.Bm, 34.80.Nz

I. INTRODUCTION

Electron elastic scattering and bremsstrahlung (a process of emission of radiation upon collision of electrons with matter) on quantum targets are important fundamental phenomena of nature with significance to both the basic and applied sciences and technologies. Yet, to date, the knowledge on these phenomena upon electron collision with such important quantum targets as endohedral fullerenes $A@C_{60}$ is largely lacking. Endohedral fullerenes, (also referred to, interchangeably, as *endohedral atoms* or just *fullerenes* in the present paper) are nanostructure formations where an atom A is encapsulated inside the hollow interior of a C_{60} fullerene. They are relatively novel and important objects of intense modern studies. In fact, the authors are aware of only one published work on the subject of low-energy electron elastic scattering off $A@C_{60}$ [1]. It is the ultimate aim of the present paper (a) to get a broader insight into properties of low-energy electron elastic scattering off $A@C_{60}$, (b) to provide the initial insight into features of electron low-frequency bremsstrahlung on $A@C_{60}$, and (c) to explore to a greater extent how said properties and features might evolve with changing the size, softness, and spin of the encapsulated atom. To meet this goal, the authors pick typical representatives of atoms from the family of noble gases (Ar and Xe), $3d$ transition metals (Cr and Mn), and alkaline (Ba) and rare-earth (Eu) elements of the periodic table. As a result, the basic features as well as characteristic similarities and discrepancies of electron elastic scattering and low-frequency bremsstrahlung on various endohedral fullerenes $A@C_{60}$ are revealed, interpreted, and detailed within the framework of the model.

The interaction of radiation and charged particles with endohedral atoms is a complicated multifaceted process. This is in view of a great variety of various effects that contribute to the process. It is, therefore, both desirable and important to understand how each of the "facets" contributes to and results in this or that effect in the processes of interest, rather than to get only the cumulative result. In the present paper, we bring to light the impact of a "static facet" on $e + A@C_{60}$ elastic scattering and bremsstrahlung. This is achieved by considering these processes in the framework of an approximation referred to as the *model static-exchange approximation* in the present paper. In this approximation, the C_{60} cage is modeled by an attractive spherical annular-potential well $U_c(r)$ of certain inner radius r_0, width Δ, and depth U_0. The C_{60} cage, thus, is regarded as a nonpolarizable target. The encapsulated atom A is positioned at the center of the potential $U_c(r)$ and is regarded as a nonpolarizable target as well. The potential of $A@C_{60}$ is defined as the sum of the potential $U_c(r)$ and nonlocal Hartree-Fock (HF) potential of the encapsulated atom A. The corresponding HF equation is then solved in order to determine the wave functions and electron elastic-scattering phase shifts upon $e + A@C_{60}$ collision. Note that this approximation, where the C_{60} is modeled by the the potential $U_c(r)$ with the atom A being at the center of the potential, has been used for the study of the interaction of photons and charged particles with endohedral fullerenes $A@C_{60}$ on numerous occasions; see, e.g., [1–6] (and references therein). Also, the replacement of the C_{60} cage by the same potential $U_c(r)$ was employed in work [7] for the study of electron elastic scattering off empty C_{60} as well. In the same work, the study of $e + C_{60}$ scattering was paralleled by the calculation performed in the framework of a sophisticated *ab initio* molecular-Hartree-Fock approximation combined with the Schwinger multichannel scattering theory. The work [7] provided a thorough, detailed comparison of calculated results for the $e + C_{60}$ scattering phase shifts as well as partial and total elastic-scattering cross sections obtained in the frameworks of these two approximations. A reasonable qualitative, and even semiquantitative, agreement between some of the most prominent features of $e + C_{60}$ elastic scattering, predicted by the two calculations, was demonstrated. Such agreement speaks in favor of the overall usability of the U_c-model-potential approximation to electron-fullerene collision.

In the present work, the electron collision energy ϵ is assumed to be sufficiently small ($\epsilon \leqslant 15$ eV). At such energies, the electron wavelength $\lambda > 3$ Å. It, thus, exceeds noticeably the bond length $D \approx 1.44$ Å between the carbon atoms in C_{60}. Correspondingly, the incoming electrons will "see" the C_{60} cage as a homogeneous rather than "granular" cage. This justifies the modeling of the C_{60} cage by a smooth potential,

in general, such as the above introduced potential $U_c(r)$, in particular. Furthermore, in the present work, the emphasis is on low-frequency bremsstrahlung, $\omega \to 0$. In the latter case, (a) the bremsstrahlung phenomenon can easily be attacked in the framework of a low-frequency approximation [8] and (b) the contribution of a tricky "polarization bremsstrahlung" amplitude [9–11] (and references therein) can be safely excluded from the study. (The "polarization bremsstrahlung" amplitude is the amplitude of the photon emission by a target during its dynamical polarization by an incoming electron.)

Thus, the model static-exchange approximation employed in the present paper for the study of both low-energy electron elastic scattering and low-frequency bremsstrahlung upon $e + A@C_{60}$ collision is overall reasonable. It has, however, obvious drawbacks such as the omission of accounting for electron correlation in and polarization by an incident electron of an $e + A@C_{60}$ system. It also leaves out of consideration various molecular effects associated with the g and u parity of molecular terms, LUMO and HOMO molecular orbitals, σ-bound and π-unbound orbitals, etc. A thorough discussion of the impact of these molecular-structure effects on electron elastic scattering off empty C_{60}, resulting in the prediction of resonances, in particular, $\pi*$-shape resonances, neither of which can be accounted for in the framework of the simple model static-exchange approximation, is given in Ref. [7], to which the reader is referred for details. Obviously, the case of electron collision with a "stuffed" C_{60}, i.e., $A@C_{60}$, is even more complicated than the case of $e + C_{60}$ scattering; the development of a corresponding comprehensive theory is for future years. Therefore, in order to understand, interpret, and appreciate the impacts of omitted effects on $e + A@C_{60}$ elastic scattering and bremsstrahlung, one *does* need to know how the processes develop without accounting for such effects. The present study is an attempt to provide researchers with such knowledge. Moreover, the model static-exchange approximation allows one to uncover characteristic properties of the investigated phenomena which do not depend on the actual molecular structure of C_{60} cage. The present work discusses some of the most basic intrinsic properties of low-energy electron elastic scattering and electron low-frequency bremsstrahlung off $A@C_{60}$ fullerenes. It identifies the most interesting and/or useful future measurements or more rigorous calculations to be performed in order to advance this field of study.

Finally, the present study also has a significance which is independent of its direct applicability to endohedral fullerenes. This is because it falls into a mainstream of intensive modern studies where numerous aspects of the structure and spectra of atoms under various kinds of confinements are being attacked from many different angles by research teams worldwide. This has resulted in a huge array of unraveled effects and data being accumulated in a large number of publications; see reviews [2,12–16] (and references therein). There, one finds a wealth of information on properties of single-electron, two-electron, and many-electron atoms confined by impenetrable spherical, spheroidal, as well as open boundary potentials (e.g., see review papers in [14] by Aquino, p. 123; Laughlin, p. 203; Cruz, p. 255; Garza and Vargas, p. 241), oscillator potentials (e.g., Patil and Varshni [14], p. 1), potentials limited by conoidal boundaries (Ley-Koo [14], p. 79), Debye potentials (Sil, Canuto, and Mukherjee [15], p. 115), fullerene-cage potentials (Dolmatov [15], p. 13; Charkin *et al.* [15], p. 69; Amusia *et al.* [17]), potential with dihedral angles (Ley-Koo and Sun [16], p. 1), etc. The results of the present study add basic knowledge to the collection of atomic properties under confinement as well.

II. THEORY

In the present work, the C_{60} cage is modeled by a spherical annular-potential well, $U_c(r)$:

$$U_c(r) = \begin{cases} -U_0, & \text{if } r_0 \leqslant r \leqslant r_0 + \Delta, \\ 0, & \text{otherwise.} \end{cases} \quad (1)$$

Here, r_0, Δ, and U_0 are the inner radius, thickness, and depth of the potential well, respectively; their magnitudes are borrowed from Ref. [7]. Namely, $\Delta = 2.9102\ a_0$ (a_0 being the first Bohr radius of the hydrogen atom), $r_0 = R_c - (1/2)\Delta = 5.262\ a_0$ ($R_c = 6.7173\ a_0$ being the radius of the C_{60} skeleton), and $U_0 = 7.0725$ eV (found by matching the electron affinity $EA = -2.65$ eV of C_{60} with the assumption that the orbital momentum of the 2.65-eV state is $\ell = 1$). These values of the adjustable parameters are most consistent with the corresponding observations.

Next, the wave functions $\psi_{n\ell m_\ell m_s}(\boldsymbol{r},\sigma) = r^{-1}P_{nl}(r)Y_{lm_\ell}(\theta,\phi)\chi_{m_s}(\sigma)$ and binding energies ϵ_{nl} of atomic electrons (n, ℓ, m_ℓ, and m_s is the standard set of quantum numbers of an electron in a central field; σ is the electron spin coordinate) are the solutions of a system of the "endohedral" HF equations [in atomic units (a.u.)]:

$$\left[-\frac{\Delta}{2} - \frac{Z}{r} + U_c(r)\right]\psi_i(\boldsymbol{x}) + \sum_{j=1}^{Z}\int \frac{\psi_j^*(\boldsymbol{x}')}{|\boldsymbol{x} - \boldsymbol{x}'|} \times [\psi_j(\boldsymbol{x}')\psi_i(\boldsymbol{x}) - \psi_i(\boldsymbol{x}')\psi_j(\boldsymbol{x})]d\boldsymbol{x}' = \epsilon_i\psi_i(\boldsymbol{x}). \quad (2)$$

Here, Z is the nuclear charge of the atom, $\boldsymbol{x} \equiv (\boldsymbol{r},\sigma)$, and the integration over $\boldsymbol{x}$ implies both the integration over $\boldsymbol{r}$ and summation over σ. Equation (2) differs from the ordinary HF equation for a free atom by the presence of the $U_c(r)$ potential in the equation. This equation is first solved in order to calculate the electronic ground-state wave functions of the encapsulated atom. Once the electronic ground-state wave functions are determined, they are plugged back into Eq. (2) in place of the $\psi_j(\boldsymbol{x}')$ and $\psi_j(\boldsymbol{x})$ functions in order to calculate the electronic wave functions of scattering states $\psi_i(\boldsymbol{x})$ and their radial parts $P_{\epsilon_i\ell_i}(r)$. The corresponding electron elastic-scattering phase shifts $\delta_\ell(k)$ are then determined by referring to $P_{k\ell}(r)$ at large r [18]:

$$P_{k\ell}(r) \to \sqrt{\frac{2}{\pi}}\sin\left(kr - \frac{\pi\ell}{2} + \delta_\ell(k)\right). \quad (3)$$

Here, k is the electron's wave number [$k \equiv |\boldsymbol{k}| = (2m\epsilon/\hbar^2)^{1/2}$, $\boldsymbol{k}$ and m being the electron's wave vector and mass, respectively]; $P_{k\ell}(r)$ is normalized to $\delta(k - k')$, where k and k' are the wave numbers of the incident and scattered electrons, respectively. The total electron elastic-scattering cross section $\sigma_{el}(\epsilon)$ is then found in accordance with the well-known formula

for electron scattering by a central-potential field [18]:

$$\sigma_{\rm el}(k) = \frac{4\pi}{k^2}\sum_{\ell=0}^{\infty}(2\ell+1)\sin^2\delta_\ell(k). \quad (4)$$

A differential cross section $d\sigma(\omega)$ of bremsstrahlung into the frequency interval $d\omega$, the direction of the photon momentum $\mathbf{p}_{ph} = \hbar\boldsymbol{q}$ into the solid angle $d\Omega_{\boldsymbol{q}}$, and the direction of the momentum $\mathbf{p}' = \hbar\boldsymbol{k}'$ of a scattered electron into $d\Omega_{\boldsymbol{k}'}$ are defined as follows [19]:

$$d\sigma(\omega) = \frac{m^2e^2q^3k'}{(2\pi)^4\hbar^3k} \times \left|\hat{\boldsymbol{e}}_q\int(\psi^+_{\boldsymbol{k}})^*\boldsymbol{r}\psi^-_{\boldsymbol{k}'}d\boldsymbol{r}\right|^2 d\omega d\Omega_{\boldsymbol{q}}d\Omega_{\boldsymbol{k}'}. \quad (5)$$

Here, $\hbar qc = \hbar\omega = \frac{\hbar^2k^2}{2m} - \frac{\hbar^2k'^2}{2m}$, where c is the speed of light, e is the electronic charge, $\boldsymbol{k}'$ is the wave vector of the scattered electron, $\hat{\boldsymbol{e}}_q$ is the unit vector of the photon polarization, and $\psi^{\pm}_{\boldsymbol{k}}$ are the wave functions of the incident and scattered electrons, respectively:

$$\psi^{\pm}_{\boldsymbol{k}}(\boldsymbol{r}) = \frac{(2\pi)^{3/2}}{k}\sum_{\ell,\mu}i^\ell\exp[\pm i\delta_\ell(k)] \times Y^*_{\ell m_\ell}(\theta_{\boldsymbol{k}},\phi_{\boldsymbol{k}})Y_{\ell m_\ell}(\theta_{\boldsymbol{r}},\phi_{\boldsymbol{r}})\frac{P_{k\ell}(r)}{r}. \quad (6)$$

In the above equation, $\theta_{\boldsymbol{k}}$ and $\phi_{\boldsymbol{k}}$ are the spherical angles of the electron wave vector $\boldsymbol{k}$, whereas $\theta_{\boldsymbol{r}}$ and $\phi_{\boldsymbol{r}}$ are the spherical angles of the electron position vector $\boldsymbol{r}$.

Let us position the origin of a rectangular XYZ system of coordinates on the encapsulated atom A. Let us assume that the momentum $\boldsymbol{p} = \hbar\boldsymbol{k}$ of an incident electron lies along the Z axis, pointing in its positive direction. Furthermore, in the final state of the system, let us measure the directions of both the momentum $\boldsymbol{p}_{\rm ph} = \hbar\boldsymbol{q}$ of an emitted photon and its polarization vector $\hat{\boldsymbol{e}}_q$. The vector $\hat{\boldsymbol{e}}_q$ will be determined relative to a $(\boldsymbol{p},\boldsymbol{p}_{ph})$ plane, being either parallel $(\boldsymbol{e}_{q\parallel})$ or perpendicular $(\boldsymbol{e}_{q\perp})$ to the plane. Then, with the help of Eq. (5), one can determine the corresponding differential cross sections $d\sigma^{\perp}/d\omega d\Omega_{\boldsymbol{q}}$ and $d\sigma^{\parallel}/d\omega d\Omega_{\boldsymbol{q}}$ into the unit intervals of ω and $\Omega_{\boldsymbol{q}}$:

$$\frac{d\sigma^{\perp}}{d\omega d\Omega_{\boldsymbol{q}}} = \frac{1}{8\pi}\frac{d\sigma}{d\omega}\left[1-\frac{1}{2}\beta(\omega)\right], \quad (7)$$

$$\frac{d\sigma^{\parallel}}{d\omega d\Omega_{\boldsymbol{q}}} = \frac{1}{8\pi}\frac{d\sigma}{d\omega}\left\{1+\frac{1}{2}\beta(\omega)[1-2P_2(\cos\theta)]\right\}. \quad (8)$$

Here, $P_2(\cos\theta)$ is the Legendre polynomial of the second order, θ is the angle between the Z axis and the photon momentum $\boldsymbol{p}_{ph}$, $d\sigma/d\omega$ is the bremsstrahlung angle-integrated cross section (or, interchangeably, the spectral density of bremsstrahlung) [19], and $\beta(\omega)$ is the angular-asymmetry parameter of bremsstrahlung:

$$\frac{d\sigma}{d\omega} = \frac{8\pi^2}{3}\frac{m^2\hbar^4\alpha^3}{\mathrm{e}^4}\frac{\omega^3}{p'p^3} \times\sum_{\ell=0}^{\infty}\left[\ell D^2_{\ell-1}(p)+(\ell+1)D^2_{\ell+1}(p)\right], \quad (9)$$

$$\beta(\omega) = \left[\sum_{\ell=0}^{\infty}\left(\ell D^2_{\ell-1}+(\ell+1)D^2_{\ell+1}\right)\right]^{-1} \times\sum_{\ell=0}^{\infty}(2\ell+1)^{-1}\big[(\ell+1)(\ell+2)D^2_{\ell+1} +\ell(\ell-1)D^2_{\ell-1}-6\ell(\ell+1)D_{\ell+1}D_{\ell-1} \times\cos(\delta_{\ell+1}-\delta_{\ell-1})\big]. \quad (10)$$

Here, α is the fine-structure constant and $D_{\ell\pm1}$ is the bremsstrahlung dipole amplitude:

$$D_{\ell\pm1} = \int_0^{\infty}P_{k',\ell\pm1}rP_{k,\ell}(r)dr. \quad (11)$$

To determine the differential cross section $d\sigma/d\omega d\Omega_{\boldsymbol{q}}$ of unpolarized bremsstrahlung, one adds Eqs. (7) and (8) together and arrives at the known formula (see, e.g., [20]):

$$\frac{d\sigma}{d\omega d\Omega_{\boldsymbol{q}}} = \frac{1}{4\pi}\frac{d\sigma}{d\omega}\left[1-\frac{1}{2}\beta(\omega)P_2(\cos\theta)\right], \quad (12)$$

where the parameter $\beta(\omega)$ is given by the same Eq. (10).

Next, the parameter of the degree of the bremsstrahlung's polarization, ζ_3 (known as the Stokes third parameter), defined as the ratio of the difference between $d\sigma^{\perp}(\omega)/d\omega d\Omega$ and $d\sigma^{\parallel}(\omega)/d\omega d\Omega$ to their sum, takes the following form:

$$\zeta_3(\theta) = \frac{\beta[1-P_2(\cos\theta)]}{2-\beta P_2(\cos\theta)}. \quad (13)$$

In the framework of the low-frequency bremsstrahlung approximation ($\omega\to0$), utilized in the present paper, $\epsilon_{\rm i}\approx\epsilon_{\rm f}$ ($\epsilon_{\rm i}$ and $\epsilon_{\rm f}$ are the initial and final electron energy, respectively). In this case, the functions $P_{k,\ell}(r)$ and $P_{k'\ell\pm1}$ in Eq. (11) can [8] be replaced by their asymptotic forms, Eq. (3). Correspondingly, one readily obtains (see, e.g., [8,20])

$$D_{\ell\pm1}(\omega)|_{\omega\to0} = \pm\frac{1}{\pi}\left(\frac{p}{m\omega}\right)^2\sin[\delta_\ell(p)-\delta_{\ell\pm1}(p)]. \quad (14)$$

As was noted in the previous section, some of the encapsulated atoms of interest are Cr, Mn, and Eu. Theses are high-spin atoms, owing to one or two semifilled subshells in their ground-state configurations: Cr($...3d^54s^1$, ^7S) (with the two semifilled subshells $3d^5$ and $4s^1$), Mn($...3d^54s^2$, ^6S) (with the single semifilled subshell $3d^5$), and Eu($...4f^76s^2$, ^8S) (with the single semifilled subshell $4f^7$). Atoms with open as well as semifilled subshells require a special approach to the calculation of their structure and spectra. A convenient, effective theory to calculate the structure of a semifilled shell atom is the "spin-polarized" Hartree-Fock (SPHF) approximation developed by Slater [21]. The quintessence of SPHF is as follows. It accounts for the fact that spins of all electrons in the semifilled subshell(s) of the atom (e.g., in the $3d^5\uparrow$ and $4s^1\uparrow$ subshells in the Cr atom) are co-directed, in accordance with Hund's rule, say, all pointing upward. This results in splitting of each of other closed $n\ell^{2(2\ell+1)}$ subshells in the atom into two semifilled subshells of opposite spin orientations, $n\ell^{2\ell+1}\uparrow$ and $n\ell^{2\ell+1}\downarrow$. This is in view of the presence of exchange interaction between $nl\uparrow$ electrons with only spin-up electrons in the original spin-unpaired semifilled subshell(s) of the atom (such as the $3d^5\uparrow$ and $4s^1\uparrow$ subshells in the Cr

atom) but absence of such for $nl\downarrow$ electrons. Thus, the SPHF configurations of the picked-out semifilled-subshell atoms are as follows:

Cr$(...3p^3\uparrow 3p^3\downarrow 3d^5\uparrow 4s^1\uparrow, {}^7S)$,
Mn$(...3p^3\uparrow 3p^3\downarrow 3d^5\uparrow 4s^1\uparrow 4s^1\downarrow, {}^6S)$,
Eu$(...4d^5\uparrow 4d^5\downarrow 4f^7\uparrow 6s^1\uparrow 6s^1\downarrow, {}^8S)$.

SPHF equations for the ground state, bound excited states, and scattering states of a semifilled shell atom differ from ordinary HF equations for closed-shell atoms by accounting for exchange interaction only between electrons with the same spin orientation ($\uparrow,\uparrow$ or $\downarrow,\downarrow$). To date, SPHF has successfully been extended to studies of electron elastic scattering off isolated semifilled shell atoms in a number of works [22–24] (and references therein). In the present paper, SPHF is utilized for calculation both of the atomic and scattering states of $A@C_{60}$ endohedral fullerenes, where A is a semifilled shell atom.

III. RESULTS AND DISCUSSION

A. Valence orbitals of the encapsulated atoms A in $A@C_{60}$

The impact of the C_{60} cage on the valence orbitals of the encapsulated atoms of interest is illustrated in Fig. 1. Note that the free-Ar $3p$ valence orbital practically coincides with the Ar@C_{60} $3p$ orbital. Even the $5p$ valence orbital of a bigger Xe atom is only insignificantly altered upon its encapsulation inside the C_{60} cage. Therefore, these atoms are referred to as the "compact" atoms in the present paper. In contrast, the valence orbitals of the Ba as well as Cr, Mn, and Eu atoms are significantly drawn into the potential well, i.e., into the region of the wall of C_{60}. These atoms are to be referred to as the "soft" atoms.

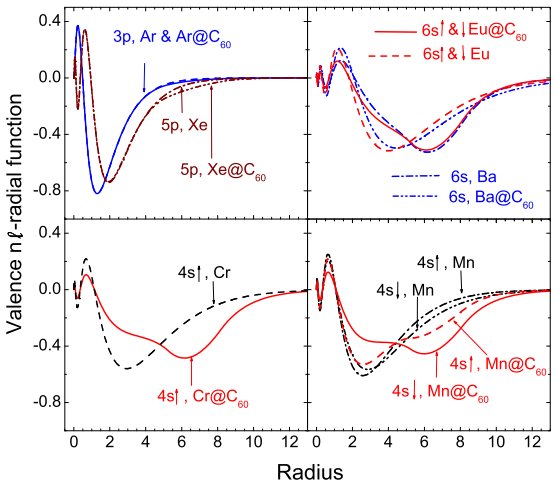

FIG. 1. (Color online) Calculated $P_{ns\uparrow}(r)$ and $P_{ns\downarrow}(r)$ radial functions (in atomic units) of the valence subshells of closed-shell Ar@C_{60}, Xe@C_{60}, and Ba@C_{60} atoms, as well as semifilled-shell Cr@C_{60}, Mn@C_{60}, and Eu@C_{60} along with those of their free counterparts, as marked, versus radius (in units of a_0, a_0 being the first Bohr radius); the spatial region $5.262 < r < 8.17$ belongs to the wall of the C_{60} cage. Note, in Eu@C_{60}, the $6s\uparrow$ and $6s\downarrow$ orbitals are drawn into the C_{60} cage equally strongly (see text) and are, thus, totally blended with each other in the plotted figure.

Next, note that the $4s\downarrow$ orbital of Mn is drawn into the C_{60} wall noticeably stronger than the $4s\uparrow$ orbital. This induces the transfer of a noticeable part of primarily the *spin-down* electron density from the encapsulated atom to the C_{60} cage. Correspondingly, the C_{60} cage becomes, as it were, "charged" by a *spin-down* electron density. This effect was originally spotted in Mn@C_{60} [1], where it was named the "C_{60}-spin-charging effect." Later, it was detailed on a more extensive scale with an eye on the register of a quantum computer in Ref. [25]. In contrast to Mn@C_{60}, the cage becomes *spin-up* charged in Cr@C_{60}. This is because of a significant *spin-up* electron density drain from a $4s\uparrow$ spin-unpaired semifilled subshell of Cr to the C_{60} cage. In contrast, the spin-dependent drain of the valence electron density does not take place in Eu@C_{60}. This is because the $6s\uparrow$ and $6s\downarrow$ orbitals are drawn into the C_{60} cage equally. The latter, in turn, is because the $4f^7\uparrow$ semifilled subshell of Eu lies much deeper relative to its $6s^1\uparrow$ and $6s^1\downarrow$ subshells than the spin-unpaired semifilled $3d^5\uparrow$ subshell of Mn relative to its spin-up and spin-down $4s$ subshells. Correspondingly, the exchange interaction between the $4f\uparrow$ and $6s\uparrow$ electrons in Eu is negligible, and there is no exchange interaction between the $4f\uparrow$ and $6s\downarrow$ electrons. Hence, there is practically no difference between the $6s\uparrow$ and $6s\downarrow$ orbitals of free or encapsulated Eu. As a result, the C_{60} cage in Eu@C_{60} is "spin neutral." Note that, as was argued in Ref. [25], the C_{60} spin charging can affect the manipulation of spins in the corresponding $A@C_{60}$ systems and that it must inhibit, or at least render more complex, the operation of the register of a fullerene-based quantum computer [26].

The above findings stir up one's mind by way of wondering (a) how sensitive is electron elastic scattering and bremsstrahlung to the *size* of a *compact* encapsulated atom? (b) alternatively, how sensitive are these phenomena to the *size* of a *soft* encapsulated atom? and (c) how sensitive are these phenomena to the *spin* of an encapsulated atom? The rest of the present work is motivated by the search for answers to these questions.

B. Electron collision with a closed shell $A@C_{60}$: $A = Ar, Xe, Ba$

1. *Electron elastic-scattering and bremsstrahlung cross sections*

Calculated total electron elastic-scattering cross sections $\sigma_{el}^{A@C_{60}}$, bremsstrahlung cross section $\omega d\sigma/d\omega$, bremsstrahlung angular-asymmetry parameter $\beta(\epsilon)$, and Stokes polarization parameter $\zeta_3(\epsilon)|_{\theta=90^\circ}$ of low-frequency bremsstrahlung due to electron collision with Ar@C_{60}, Xe@C_{60}, Ba@C_{60}, and empty C_{60} are depicted in Fig. 2. This figure clearly demonstrates that all of the above electron elastic-scattering and bremsstrahlung quantities develop a resonance behavior. The interpretation of the oscillatory behavior of the electron elastic scattering off *empty* C_{60} was provided in Refs. [7,17]. There, it was shown that it is due to quasidiscrete states formed by a centrifugal potential barrier for the states with $\ell \geqslant 3$. Namely, the first narrow resonance in $\sigma_{el}^{C_{60}}$ at $\epsilon \approx 0.27$ eV is the f-virtual resonance, the second resonance (at $\epsilon \approx 2.3$ eV) is the g-virtual resonance, and so on. As for the s-, p-, and d-scattering states, they cannot and do not have a resonance behavior, because the model spherical-annular potential, as well as the model δ potential

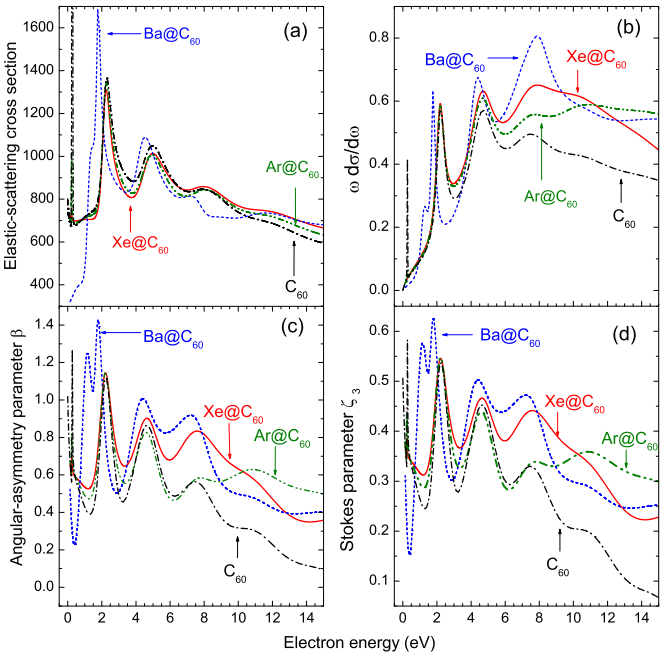

FIG. 2. (Color online) Calculated HF (a) total electron elastic-scattering cross sections $\sigma_{\rm el}^{A@C_{60}}$ and $\sigma_{\rm el}^{C_{60}}$ (in units of a_0^2), (b) bremsstrahlung cross section $\omega\frac{d\sigma}{d\omega}$ [in units of kilobarns (kb); 1 barn $= 10^{-24}$ cm^2 $\approx 3.57\times10^{-8}\ a_0^2$], (c) bremsstrahlung angular asymmetry parameter β, and (c) bremsstrahlung Stokes polarization parameter ζ_3 (at $\theta = 90^\circ$) upon electron collision with $A@C_{60}$ ($A =$ Ar, Xe, and Ba) and empty C_{60}, as marked. Note, the calculated in the present work $\sigma_{\rm el}^{C_{60}}$ coincides naturally with that calculated in Ref. [7] (not plotted in the figure) in the framework of the same model static-exchange approximation.

of work [17], was found to form an s-, p-, and d-bond state; thus the corresponding quasiresonances cannot be formed [18]. The resonance structures in bremsstrahlung quantities upon electron collision with *empty* C_{60} calculated in this work admit, naturally, the same interpretation as well.

However, the case of electron collision with *endohedral fullerenes* $A@C_{60}$ appears to not always be developing in the same way as electron collision with empty C_{60}. For example, on the one hand, the electron elastic-scattering cross sections $\sigma_{\rm el}^{Ar@C_{60}}$ and $\sigma_{\rm el}^{Xe@C_{60}}$ practically do not differ either from each other or from $\sigma_{\rm el}^{C_{60}}$. Their resonance structure, thus, admits the same interpretation as the resonance structure of $\sigma_{\rm el}^{C_{60}}$. This is because the Ar and Xe atoms are compact; i.e., their electron density is concentrated practically entirely inside the C_{60} cage, so that they are largely "shielded" by the C_{60} cage from the "attention" of the incoming electrons. On the other hand, the cross section $\sigma_{\rm el}^{Ba@C_{60}}$ behaves clearly much differently than $\sigma_{\rm el}^{C_{60}}$, or $\sigma_{\rm el}^{Ar@C_{60}}$, or $\sigma_{\rm el}^{Xe@C_{60}}$. Indeed, in $\sigma_{\rm el}^{Ba@C_{60}}$, (a) the low-energy f-virtual resonance is absent, (b) there is a sign of a new resonance near $\epsilon \approx 1.4$ eV (the latter is particularly clearly resolved in the calculated bremsstrahlung parameters), and (c) there is a noticeable dip in this cross section near 8 eV. The Ba atom was found to be a soft atom whose valence electron density is noticeably drawn into the C_{60} cage, so that the above noted peculiarities in electron-$Ba@C_{60}$ collision definitely correlate with the softness of the atom.

The finding that electron scattering off $Ar@C_{60}$, $Xe@C_{60}$, and especially off $Ba@C_{60}$ can be significantly weaker than electron scattering off *empty* C_{60}, at ceratin electron energies [see Fig. 2(a)], deserves particular attention. In other words, the gas medium of *empty* C_{60} can be much less transparent to the incoming beam of electrons than the medium of "stuffed" C_{60} ($A@C_{60}$), at ceratin electron energies. This feels somewhat counterintuitive. This finding should be combined with another counterintuitive finding of work [1], where it was shown that electron scattering off $A@C_{60}$ can even be weaker than scattering off the atom A itself.

In conclusion, the authors emphasize that results depicted in Fig. 2 demonstrate that the bremsstrahlung parameters appear to be more sensitive to the presence of a particular atom inside C_{60} than the corresponding electron elastic-scattering cross section. Indeed, e.g., a weakly developed 1.4-eV resonance in $\sigma_{\rm el}^{Ba@C_{60}}$ is seen to be resolved much better in the bremsstrahlung parameters. In addition, whereas there are little differences between $\sigma_{\rm el}^{Ar@C_{60}}$, $\sigma_{\rm el}^{Xe@C_{60}}$, and $\sigma_{\rm el}^{C_{60}}$ in the whole energy region, the corresponding bremsstrahlung parameters for one system differ significantly from bremsstrahlung parameters for another system, particularly above approximately 4 eV. The authors attribute the reason for the "enhanced" sensitivity of low-frequency bremsstrahlung to the structure of an encapsulated atom to that fact that bremsstrahlung cross section, β, and ζ_3 depend on the difference between elastic-scattering phase shifts, thereby tying up features of both phases in, as it were, "one place." In contrast, the electron elastic-scattering cross section depends on absolute values of individual phase shifts. The above also suggests that the angle-differential scattering cross sections should also be more sensitive to the presence of the encapsulated atom A inside the C_{60} cage than the integral cross sections, for the same reason as for the bremsstrahlung parameters.

In order to understand the above established peculiarities in electron elastic scattering and bremsstrahlung off $Ar@C_{60}$, $Xe@C_{60}$, and $Ba@C_{60}$, the study of the corresponding phase shifts is in order. Results of such study are detailed below.

2. *Electron elastic-scattering phase shifts*

Calculated HF electron elastic-scattering phase shifts $\delta_\ell(\epsilon)$ due to scattering off $Ar@C_{60}$, $Xe@C_{60}$, and $Ba@C_{60}$ and, for comparison, off empty C_{60} are depicted in Fig. 3. First, let us discuss the phase shifts at $\epsilon = 0$; see Table I. In order to understand the behavior of phase shifts at $\epsilon \to 0$, let us refer to the Levinson theorem [18], which we write as follows:

$$\delta_\ell(\epsilon)|_{\epsilon\to0} \to \big(N_{n_\ell} + q_\ell\big)\pi. \tag{15}$$

Here, N_{n_ℓ} is the number of occupied states with given ℓ in the ground-state configuration of a target scatterer, whereas q_ℓ is the number of additional (if any) empty bound states with the same ℓ which can accommodate (bind) an external electron. For the *empty* C_{60} cage approximated by the annular potential, Eq. (1), $N_{n_\ell} = 0$ for all ℓ's. Therefore, from the calculated values of $\delta_\ell^{C_{60}}(0)$, Table I, one concludes that $q_\ell = 1$ for $\ell = s, p$, and d, but $q_\ell = 0$ for $\ell = f$. The implication is that the confining potential $U_{\rm c}(r)$ (or the C_{60} cage itself) has the ability to bind an electron into an s, or p, or d state; this was already

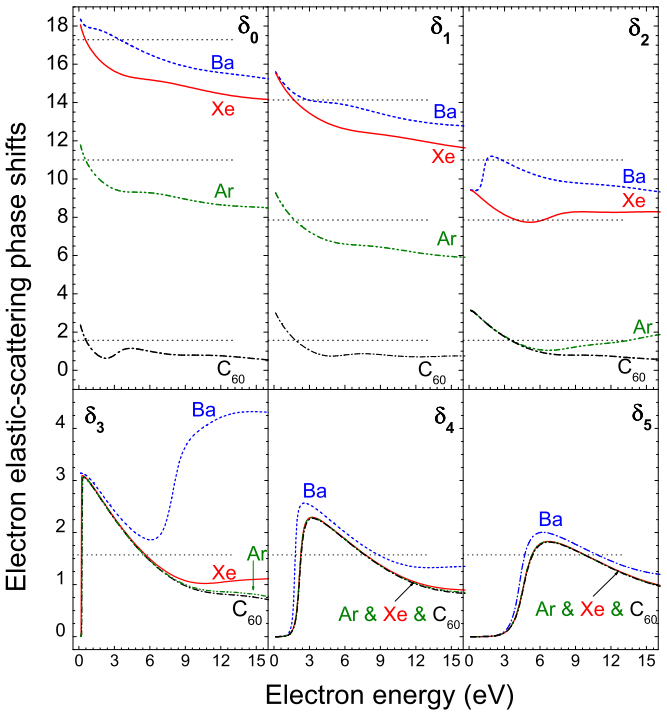

FIG. 3. (Color online) Calculated HF electron elastic-scattering phase shifts $\delta_\ell(\epsilon)$ (in units of radians) ($\ell \leqslant 5$) upon electron collision with Ar@C_{60}, Xe@C_{60}, Ba@C_{60}, and empty C_{60}, as marked. Horizontal dotted lines designate the values of δ_ℓ which are modulo $\pi/2$. For scattering off empty C_{60}, the calculated phase shifts coincide with results of Ref. [7] obtained in the framework of the identical model (not plotted in the present figure).

noted in Ref. [7]. In addition to the results of Refs. [7,17] for empty C_{60}, the present study predicts the existence of the s, p, and d anions Ar@C_{60}^- and Xe@C_{60}^-, in the given approximation. Indeed, if one counts the number of occupied s, p, and d subshells in Ar ($N_{n_\ell} = 3,2$, and 0, respectively) and Xe ($N_{n_\ell} = 5,4$, and 2, respectively), then, with the help of Eq. (15) and Table I, one easily finds that $q_s = q_p = q_d = 1$ whereas $q_f = 0$ for both atoms. For Ba@C_{60}, however, the situation is somewhat different. Indeed, as shown in Table I, $\delta_s^{\mathrm{Ba@C_{60}}}(0) = 6\pi$, and there are exactly six s subshells in the Ba atom; i.e., $N_{n_s} = 6$. This makes $q_s = 0$, for Ba@C_{60}. The latter indicates the absence of a s-bound state in the field of Ba@C_{60}. This is in contrast to the situation for Ar@C_{60}, Xe@C_{60}, and C_{60}. Next, $\delta_f^{\mathrm{Ba@C_{60}}}(0) = \pi$, although there are

TABLE I. Calculated HF electron elastic-scattering phase shifts $\delta_\ell(\epsilon)$ (at $\epsilon = 0$) upon electron collision with empty C_{60} and A@C_{60} (A = Ar,Xe, and Ba).

	$\delta_\ell(0)$			
ℓ	C_{60}	Ar	Xe	Ba
s	π	4π	6π	6π
p	π	3π	5π	5π
d	π	π	3π	3π
f	0	0	0	π

no occupied f subshells in the Ba atom. Hence, $q_f = 1$. This predicts the emergence of a f-bound state in the field of Ba@C_{60}, in contrast to the case of the Ar@C_{60}, Xe@C_{60}, and C_{60} fullerenes. Obviously, things work differently for Ba@C_{60} because of a noticeable drain of the valence electron density of Ba to the C_{60} cage; see Fig. 1.

We now discuss the energy dependence of the plotted phase shifts along with corresponding consequences in conjunction with the general scattering theory, particularly with an eye on resonance scattering. The characteristic phase-shift criterion for a low-energy quasiresonance scattering is that a phase shift $\delta_\ell(\epsilon)$ first *increases* towards modulo π with decreasing energy, then, before that value is reached, it sharply *decreases* to a zero (or another modulo π) passing through the value of, this time, modulo $\pi/2$ [18,27,28].

One can see that the f phase shifts upon electron scattering off each of the considered fullerene systems but Ba@C_{60} clearly satisfy the quasiresonance-scattering criterion. For each of the considered fullerene systems (but Ba@C_{60}), the f-phase shifts pass through the value of $\pi/2$ at about the same energy $\epsilon \approx 0.23$ eV, exactly where there is a sharp narrow resonance in the calculated corresponding electron elastic-scattering cross sections, or about where there is a narrow sharp resonance in the calculated bremsstrahlung quantities. Furthermore, the g-phase ($\ell = 4$) and h-phase ($\ell = 5$) shifts for all considered fullerene systems (the Ba@C_{60} including) clearly satisfy the quasiresonance-scattering criterion as well. One thus concludes that a low-energy resonance at $\epsilon \approx 1.76$ eV in the Ba@C_{60} collision spectra as well as the low-energy resonances at $\epsilon \approx 2.3$ eV in the spectra of other fullerenes are the quasibound resonances. The just discussed f, g, and h resonances were revealed previously in the case of electron elastic scattering off empty C_{60} in Refs. [7,17]. It is a finding of the present work that these resonances are retained in the electron collision spectra of Ar@C_{60}, Xe@C_{60}, and Ba@C_{60} (but the f resonance in Ba@C_{60}) as well. This is not entirely surprising in the framework of our model which largely neglects the interaction between the encapsulated atom and the C_{60} cage. The resonances in question occur either at very low energies or in high-ℓ electronic waves. When the energy is low, the de Broglie wavelength of the incident electron exceeds the width of the potential well and, thus, scattering is generally insensitive to details of the potential in the interior of C_{60} where an atom is encapsulated. When ℓ is big, the centrifugal barrier is too high for a low-energy high-ℓ electronic wave to penetrate deep into the interior of C_{60}, thereby making scattering of high-ℓ electronic waves generally insensitive to details of the potential as well. For Ba@C_{60}, where there is a noticeable drain of the valence electron density of Ba into the C_{60} cage, things naturally work somewhat differently. Because of the electron drain, the field of the encapsulated Ba atom becomes more attractive in the interior of C_{60}. As known [27], a stronger attractive potential increases the value of a phase shift and also moves resonances toward lower electron energy. This is why the g- and h-phase shift resonances in the case of Ba@C_{60} are greater than the corresponding resonances in the case of Ar@C_{60}, Xe@C_{60}, and C_{60}, and the resonance maxima are positioned at somewhat lower energies. Furthermore, by exploring the d-phase shift upon electron collision with Ba@C_{60}, one reveals

another finding of the present work. Namely, one can see that the low-energy behavior of the phase shift satisfies the resonance-scattering criterion as well. We thus predict the existence of (approximately) a 1.5-eV d quasiresonance in the electron collision spectrum of Ba@C_{60}. This resonance is clearly seen in the calculated bremsstrahlung spectra and, less clearly, in the calculated electron elastic-scattering cross section $\sigma_{\rm el}^{\rm Ba@C_{60}}$, Fig. 2. This 1.5-eV d quasiresonance emerges near the much stronger 1.76-eV g quasiresonance. These two resonances appear to be resolved better in the bremsstrahlung spectra than in $\sigma_{\rm el}^{\rm Ba@C_{60}}$. Next, by exploring a near-zero energy dependence of the s- and p-phase shifts depicted in Fig. 3, one can see that they pass through the value of modulo $\pi/2$ while *rising* towards modulo π at $\epsilon = 0$. Where δ_ℓ equals modulo $\pi/2$, the corresponding electron-scattering spectra maximize as well. This situation, however, should not be confused with resonance scattering, since it does not fit the resonance-scattering criterion. In accordance with the later [27], $\delta_\ell(\epsilon)$ must be *decreasing* with decreasing ϵ while passing through the value of $\pi/2$ (or modulo $\pi/2$) to a zero (or modulo π) at $\epsilon = 0$.

In conclusion, one could wonder why the s-, p-, d-, and f-phase shifts upon electron scattering off different A@C_{60} are so quantitatively different from each other even when the electron wavelength is bigger than the size of the potential well, or ℓ high, so that in both cases scattering should have been insensitive to details of the potential in the interior of C_{60}, as for the above discussed case of the g and h waves. The answer to this is simple. As known [28], exchange interaction plays an important role in electron scattering off atoms. Therefore, while the "direct" interaction between the incident electron and encapsulated atom can be shielded by the C_{60}, the exchange interaction cannot. Of particular importance is exchange interaction between an incoming electron and atomic electrons of the encapsulated atom with the same ℓ. Therefore, the more $n\ell$ subshells in the encapsulated atom with the same ℓ as the ℓ of the incoming electron, the stronger the exchange-interaction impact on the ℓ-phase shift. Thus, it is in principle impossible to make the encapsulated atom invisible to an incident electron (with the exception, perhaps, of where there are no atomic subshells with the same ℓ as the ℓ of an incident electron, as in the case of g and h scattering considered above).

3. *Independent-scattering approximation*

We now attempt to understand the differences between the d-phase shifts upon electron scattering off C_{60}, Ar@C_{60}, Xe@C_{60}, and Ba@C_{60} as well as between the f-phase shifts, Fig. 3. The noted differences are not only quantitative, but qualitative as well.

It is found in the present study that, as odious as it may seem, the above observations can be understood in terms of a simple sum of a phase shift $\delta_\ell^{\rm C_{60}}$ due to electron scattering off empty C_{60} and a phase shift δ_ℓ^A upon electron scattering by the *isolated* atom A (recently Amusia [29] came to the same conclusion as well):

$$\delta_\ell^{A@C_{60}}(\epsilon) \approx \tilde{\delta}_\ell^{A@C_{60}}(\epsilon) = \delta_\ell^A(\epsilon) + \delta_\ell^{C_{60}}(\epsilon). \qquad (16)$$

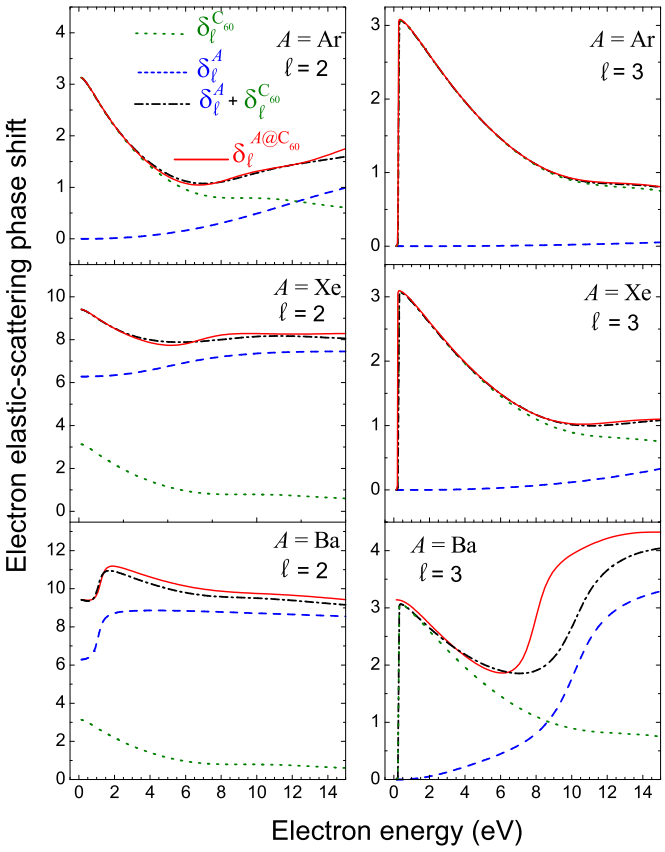

FIG. 4. (Color online) Calculated HF d- and f-phase shifts (in units of radian): dotted line, empty-C_{60} $\delta_\ell^{\rm C_{60}}$; dashed line, free-atom δ_ℓ^A; dash-dotted line, $\tilde{\delta}_\ell^{A@C_{60}} = \delta_\ell^A + \delta_\ell^{C_{60}}$; solid line, $\delta_\ell^{A@C_{60}}$ due to electron collision with A@C_{60} as the whole (true result). A = Ar,Xe,Ba.

The above stated approximation is referred to as the *independent-scattering approximation* in the present paper. Figure 4 provides the supporting evidence in favor of this approximation.

One can see from Fig. 4 that indeed $\tilde{\delta}_\ell^{A@C_{60}} \approx \delta_\ell^{A@C_{60}}$, to a good approximation. The agreement is reasonable even for the case of electron collision with Ba@C_{60}, although the latter is a less suitable system to apply this approximation to, because of the noticeable electron density drain from Ba to C_{60}. One, of course, would be too naive to expect that the independent-scattering approximation is perfect. One can readily conclude, upon exploring Fig. 4, that the characteristic differences in the d-phase shifts between $\delta_d^{\rm Ar@C_{60}}$, $\delta_d^{\rm Xe@C_{60}}$, and $\delta_d^{\rm Ba@C_{60}}$, as well as the differences in the f-phase shifts between these three systems, are due to the characteristic differences between the corresponding free-atom phase shifts δ_ℓ^A. For example, the sudden decrease (with decreasing energy) of $\delta_d^{\rm Ba@C_{60}}$ at $\epsilon \approx 1.8$ eV definitely correlates with the same for free-Ba $\delta_d^{\rm Ba}$. On the other hand, the free-Xe phase shift $\delta_d^{\rm Xe}$ behaves very much differently than $\delta_d^{\rm Ba}$. As a result, the phase shifts $\delta_d^{\rm Ba@C_{60}}$ and $\delta_d^{\rm Xe@C_{60}}$ behave nearly oppositely to each other, at low electron energies. Equally, the well-developed minimum in $\delta_f^{\rm Ba@C_{60}}$ definitely correlates with a sharp decrease (with decreasing energy) of free-Ba $\delta_f^{\rm Ba}$ from about π to a zero in

this energy region (indicative of an f-shape resonance in the f-scattering state). In contrast, the free-Ar and free-Xe f-phase shifts are a slowly changing monotonic function of energy which cannot "beat" the sharply changing empty-C_{60} f-phase shift. As a result, the $\delta_f^{\mathrm{Ba@C_{60}}}$ phase shift does, but $\delta_f^{\mathrm{Xe@C_{60}}}$ does not, develop the strong broad minimum in the discussed energy region.

The independent-scattering approximation will be frequently employed further in the paper on various occasions as an easy qualitative tool for understanding the behavior of phase shifts for other case-study systems.

C. Electron collision with high-spin A@C_{60}: A = Cr, Mn, and Eu

1. Eu@C_{60}

One of the interesting findings discussed in the previous discussion was that electron scattering off soft Ba@C_{60} has characteristic features which are absent in electron scattering off compact Ar@C_{60} and Xe@C_{60}. It is, therefore, interesting to see whether similar features will emerge in another soft A@C_{60} system, where the atom A is about as big as Ba and donates about as much of its valence electron density to C_{60} as Ba. Furthermore, it is also interesting to explore how electron scattering off such system might change if a big, soft atom A is, additionally, a high-spin atom. The ideal candidate for the stated study is the Eu@C_{60} system. Indeed, the Eu atom matches the Ba atom in the electron-density drain rate from the atom to the C_{60} cage (see Fig. 1) and, besides, Eu has the most capacious semifilled subshell, the $4f^7\uparrow$ subshell, thereby representing an atom with the highest spin. Furthermore, Eu has a spherical symmetry which simplifies greatly the corresponding calculations.

Calculated SPHF electron elastic-scattering phase shifts $\delta_{\ell\uparrow}^{\mathrm{Eu@C_{60}}}$ and $\delta_{\ell\downarrow}^{\mathrm{Eu@C_{60}}}$ of spin-up and spin-down electrons, respectively, are depicted in Fig. 5 for $\ell \leqslant 3$. Plotting phase shifts with $\ell > 3$ is not necessary since they are nearly identical to those for scattering off Ba@C_{60}. This is because a high value of the centrifugal potential barrier for these electrons makes their scattering relatively insensitive to the details of the potential inside C_{60}.

First, looking at the values of the depicted phase shifts at $\epsilon = 0$, one concludes, with the help of the Levinson theorem, that, similarly to Ba@C_{60}, the Eu@C_{60} fullerene is capable of binding an extra electron into a p, or d, or f state, but not into an s state. Furthermore, note the dependence of the phase shifts on the electron spin polarization which appears to be noticeable for the d-phase shifts but the strongest for the f-phase shifts. This spin dependence is due to the presence (absence) of exchange interaction of the spin-up $f\uparrow$ electrons of the $4f^7\uparrow$ semifilled subshell of the atom with the incident spin-up (spin-down) electrons. One can see that the f-phase shifts of oppositely spin-polarized incident electrons take even drastically different routes with decreasing electron energy.

Next, let us uncover the reason behind the most striking result—the drastic difference between the spin-up and spin-down f-phase shifts both for the free-Eu and Eu@C_{60} cases. In the framework of HF or SPHF, atoms do not make

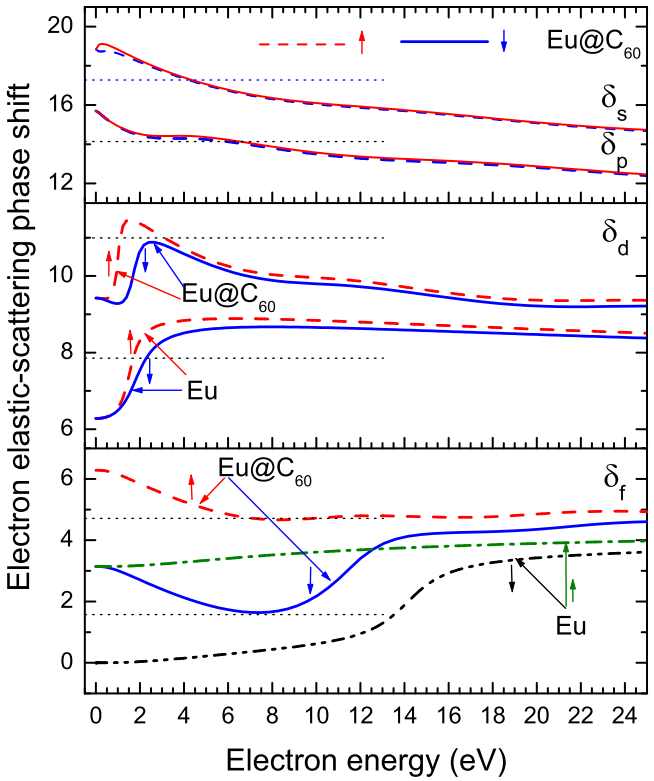

FIG. 5. (Color online) Calculated SPHF electron elastic-scattering phase shifts (in units of radians) of incident spin-down ($\downarrow$) and spin-up ($\uparrow$) electrons with $\ell \leqslant 3$ scattered off Eu@C_{60} ($\delta_{\ell\uparrow(\downarrow)}^{\mathrm{Eu@C_{60}}}$) and free-Eu $\delta_{\ell\uparrow(\downarrow)}^{\mathrm{Eu}}$, as marked. Horizontal dotted lines mark the values of δ_ℓ which are modulo $\pi/2$. The phase shifts are plotted on the expanded energy scale for a better clarity of features in the interval of 0 to 15 eV.

negative ions. Since there are no spin-down $f\downarrow$ electrons in free Eu, the free-Eu $f\downarrow$-phase shift must decrease to a zero with decreasing energy, in accordance with the Levinson theorem. This explains the calculated behavior of the free-Eu $f\downarrow$-phase shift depicted in Fig. 5. On its way to a zero, this phase shift passes through the value of $\pi/2$ at $\epsilon \approx 14$ eV, thereby causing the shape resonance in the $f\downarrow$-partial electron elastic-scattering cross section. Qualitatively, the $f\downarrow$-phase shift behaves similarly to the f-phase shift upon electron scattering off Ba; this is because Ba has no f subshells in its ground-state configuration as well. Furthermore, using the independent-scattering approximation, Eq. (16), i.e., adding the free-Eu $f\downarrow$-phase shift with the empty-C_{60} f-phase shift, one easily (no commentary is needed) arrives at the understanding of the behavior of $\delta_{f\downarrow}^{\mathrm{Eu@C_{60}}}$ as well, particularly at the understanding of the emergence of the broad minimum in $\delta_{f\downarrow}^{\mathrm{Eu@C_{60}}}$ at low electron energies. Again, all this is in a close analogy to the case of f-wave scattering off Ba@C_{60}. Let us now discuss the spin-up $f\uparrow$-phase shift. Obviously, the free-Eu $f\uparrow$-phase shift must approach the value of π, since there is the spin-up $4f^7\uparrow$ subshell in the atomic configuration of Eu. This explains the drastic difference between the free-Eu $f\downarrow$- and $f\uparrow$-phase shifts. Then, adding the free-Eu $f\uparrow$-phase shift with the empty-C_{60} f-phase shift, one arrives at the understanding of the behavior of $\delta_{f\uparrow}^{\mathrm{Eu@C_{60}}}$ depicted in the figure. In particular,

it also becomes clear why $\delta_{f\uparrow}^{\mathrm{Eu@C_{60}}} = 2\pi$ but $\delta_{f\downarrow}^{\mathrm{Eu@C_{60}}} = \pi$ at $\epsilon = 0$. As was emphasized above, the field of Eu@C_{60} binds an electron into an f state regardless of the electron spin polarization. However, since there are only $f\uparrow$-bound electrons in the free-Eu configuration, the additional binding of an f electron by the whole system Eu@C_{60} results in $\delta_{f\uparrow}^{\mathrm{Eu@C_{60}}} = 2\pi$ but $\delta_{f\downarrow}^{\mathrm{Eu@C_{60}}} = \pi$ at $\epsilon = 0$, due to the Levinson theorem.

Now, let us discuss the formation of the low-energy maxima in the d-phase shifts $\delta_{d\uparrow}^{\mathrm{Eu@C_{60}}}$ and $\delta_{d\downarrow}^{\mathrm{Eu@C_{60}}}$. Let us start from the free-atom case. In accordance with the Levinson theorem, both the free-Eu $d\uparrow$- and $d\downarrow$-phase shifts must take the value of 2π at $\epsilon = 0$, owing to the presence of two $nd^5\uparrow$ and two $nd^5\downarrow$ ($n = 3,4$) subshells in the atom. This explains why the free-Eu d-phase shifts, depicted in Fig. 5, both decrease to 2π at $\epsilon = 0$ regardless of the spin polarization of the incident d electrons. It appears that the energy dependence and low-energy position of the rapid decrease of the free-Eu spin-up and spin-down d-phase shifts, during which they pass through the value of modulo $\pi/2$, obey the quasiresonance criterion. Thus, in the case of free Eu, both the $d\uparrow$- and $d\downarrow$-partial electron elastic scattering cross sections are subject to a quasiresonance enhancement near 2 eV of the electron energy. This is in close analogy to the case of Ba. Furthermore, adding the empty-C_{60} d-phase shift to the free-Eu d-phase shifts results in $\tilde{\delta}_{d\uparrow}^{\mathrm{Eu@C_{60}}}$ and $\tilde{\delta}_{d\downarrow}^{\mathrm{Eu@C_{60}}}$ (not plotted in Fig. 5), which have a low-energy maxima that should, and they do, approximately match the low-energy maxima in actual $\delta_{d\uparrow}^{\mathrm{Eu@C_{60}}}$ and $\delta_{d\downarrow}^{\mathrm{Eu@C_{60}}}$. In other words, the above finds that the low-energy behavior of the Eu@C_{60} d-phase shifts is directly associated with the behavior of the free-Eu d-phase shifts, similar to the Ba@C_{60} case.

Moreover, the above results show clearly that only the spin-up $\delta_{d\uparrow}^{\mathrm{Eu@C_{60}}}$ phase shift satisfies the quasiresonance criterion (similar to the d scattering off Ba@C_{60}). Hence, scattering of the $d\uparrow$-electronic wave off Eu@C_{60} will be resonantly enhanced at $\epsilon \approx 1$ eV, whereas the $d\downarrow$ scattering will not. We, thus, have unraveled an interesting phenomenon the quintessence of which is that the quasiresonance trapping of an incident electronic wave can depend on its spin polarization. We term the discovered effect the *selective spin-dependent trapping effect*.

It is interesting to explore the electron elastic-scattering cross sections $\sigma_{\mathrm{el}\uparrow(\downarrow)}^{\mathrm{Eu@C_{60}}}$, low-frequency bremsstrahlung cross section $\omega d\sigma_{\uparrow(\downarrow)}/d\omega$, angular-asymmetry parameter $\beta_{\uparrow(\downarrow)}$, and Stokes polarization parameter $\zeta_3\uparrow(\downarrow)$, in general, and how the selective spin-dependent phenomenon will affect these quantities, in particular. The corresponding calculated data are depicted in Fig. 6. The peaks in $\sigma_{\mathrm{el}\uparrow}^{\mathrm{Eu@C_{60}}}$ and $\omega d\sigma_{\uparrow}^{\mathrm{Eu@C_{60}}}/d\omega$, positioned at approximately 1.9, 4.6, and 8 eV, have the same origin; i.e., they are due to the quasiresonances in the phase shifts with $\ell = 4$, 5, and 6, respectively, as in the case of empty C_{60}. The resonance peaks at about the same energies can be seen in bremsstrahlung β's and ζ_3's as well. They have the same origin as the resonances in the cross sections.

Furthermore, note that the *spin-up* elastic-scattering and bremsstrahlung cross sections maximize, additionally, at

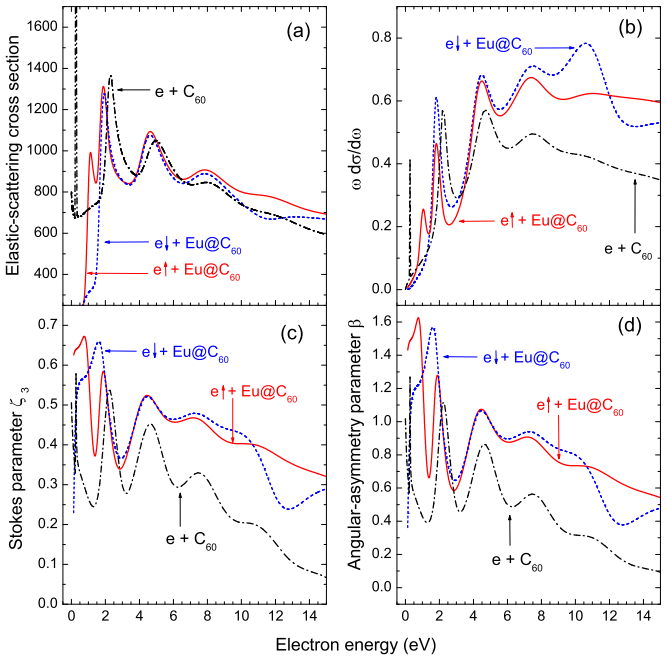

FIG. 6. (Color online) Calculated SPHF (a) total electron elastic-scattering cross sections $\sigma_{\mathrm{el}\uparrow(\downarrow)}$ (in units of a_0^2), (b) bremsstrahlung cross sections $\omega\frac{d\sigma_{\uparrow(\downarrow)}}{d\omega}$ (in units of kb), (c) bremsstrahlung angular-asymmetry parameter $\beta_{\uparrow(\downarrow)}$, and (c) Stokes polarization parameter $\zeta_3\uparrow(\downarrow)|_{\theta=90^\circ}$ upon collision of spin-up and spin-down incident electrons with Eu@C_{60} and empty C_{60}, as marked.

$\epsilon \approx 1.1$ eV as well. This is due to the quasiresonance in the $d\uparrow$-phase shift induced by the selective spin-dependent trapping effect discussed above. The corresponding difference between spin-up and spin-down β's and ζ_3's is even more drastic than in the case of the cross sections, near 1 eV.

In addition, explore the energy region between 10 and 12 eV. There is an additional strong difference between the calculated spin-up and spin-down quantities; the difference looks especially impressive for the case of bremsstrahlung cross sections. This difference is due to the peculiarity in the $f\downarrow$-phase shift, namely due to the above discussed shape resonance in there.

Finally, note that, similarly to the case of Ba@C_{60}, one encounters, once again, a counterintuitive result where electron elastic scattering off Eu@C_{60} is much *weaker* than off empty C_{60}, at certain electron energies.

2. Cr@C_{60} *and* Mn@C_{60}

Although in the above case of Eu@C_{60} we dealt with the atom which is both a big-sized and high-spin atom, an important nuance associated with atomic spin was missing. Namely, in Eu@C_{60}, the C_{60} is not spin charged, because both the $6s\uparrow$- and $6s\downarrow$-electron densities are drawn into the C_{60} cage equally strongly. Good candidates to account both for the impact of a high atomic spin and C_{60} spin charging on electron collision with A@C_{60} are the two closest atom neighbors in the periodic table—the Cr($...3d^5\uparrow 4s^1\uparrow$, ^7S) ($Z = 24$) and Mn($...3d^5\uparrow 4s^1\uparrow 4s^1\downarrow$, ^6S) ($Z = 25$) atoms. Moreover, this pair of atoms is interesting in that the Cr atom makes the C_{60}

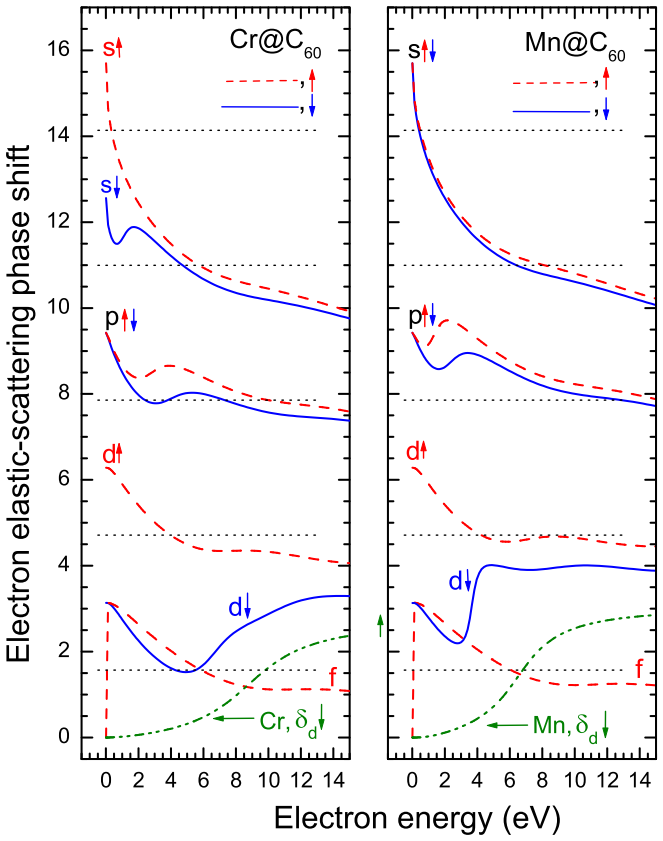

FIG. 7. (Color online) Calculated SPHF spin-down (solid lines) and spin-up (dashed lines) s-, p-, d-, and f-phase shifts (in units of radians) upon electron collision with $Cr@C_{60}$, free-Cr (dash-dot-dot) (left column), as well as $Mn@C_{60}$ and free-Mn (dash-dot-dot) (right column), as marked. For the f-phase shifts, only the $f\uparrow$-phase shift is plotted in view of a near identity between these spin-up and spin-down phase shifts. The phase shifts with $\ell > 3$ are practically identical to those for electron-C_{60} collision and not plotted on the figure.

primarily spin-up charged, whereas the Mn atom makes it primarily spin-down charged, as was discussed earlier in the paper. It is, therefore, interesting to study electron elastic scattering and bremsstrahlung off $Cr@C_{60}$ and $Mn@C_{60}$ and intercompare results obtained.

SPHF-calculated electron elastic-scattering phase shifts of spin-up and spin-down electrons with $\ell \leqslant 3$ due to collision with $Cr@C_{60}$ or $Mn@C_{60}$ are depicted in Fig. 7. First, note the values of s-, p-, and d-phase shifts at $\epsilon = 0$. These values, in conjunction with the SPHF ground-state configurations of Cr and Mn as well as the Levinson theorem, speak to that fact that the model static-exchange potentials of $Cr@C_{60}$ and $Mn@C_{60}$ support a spin-up and spin-down s-bound state, p-bound state, and d-bound state beyond the atomic configurations of the Cr and Mn atoms themselves. Both potentials, however, do not support bound states with $\ell \geqslant 3$. The binding properties of $Cr@C_{60}$ and $Mn@C_{60}$ are, thus, the same as the binding properties of compact $Ar@C_{60}$ and $Xe@C_{60}$.

Second, note how differently the s-phase shift $\delta_{s\downarrow}^{Cr@C_{60}}$ behaves compared to $\delta_{s\uparrow}^{Cr@C_{60}}$, $\delta_{s\uparrow}^{Mn@C_{60}}$, and $\delta_{s\downarrow}^{Mn@C_{60}}$ at low energies. While the behavior of the three latter phase shifts is typical for the case of low-energy scattering on an s-discrete level of small binding energy, the behavior of the spin-down phase shift $\delta_{s\downarrow}^{Cr@C_{60}}$ is not; it breaks the rule at $\epsilon \approx 1.7$ eV. This is another bright example of the role of exchange interaction in electron scattering off a multielectron atom encapsulated inside a confining potential (the C_{60} potential). Indeed, the major difference between the $s\uparrow$ and $s\downarrow$ scattering off $Cr@C_{60}$ is the presence of exchange interaction between the $s\uparrow$-incident electron and the only spin-unpaired valence $4s\uparrow$ electron in encapsulated Cr, but the absence of exchange interaction between this valence electron and an $s\downarrow$-incident electron. Because of this [and in conjunction with the Levinson theorem, Eq. (15)], the free-Cr $s\downarrow$-phase shift $\delta_{s\downarrow}^{Cr}$ [23] starts, at $\epsilon \approx 0.3$ eV, sharply decreasing to the value of $\delta_{s\downarrow}^{Cr}(0) = 3\pi$. It is clear then, on the basis of the independent-scattering approximation, that the $\delta_{s\downarrow}^{Cr@C_{60}}$ phase shift must start first decreasing but then increasing with decreasing energy, reaching the value of $\delta_{s\downarrow}^{Cr@C_{60}}(0) = 4\pi$ (because $Cr@C_{60}$ supports an $s\downarrow$-bound state), exactly as depicted in Fig. 7. There is some interesting difference, though, between the sharp decrease of the free-Cr $\delta_{s\downarrow}^{Cr}$ and $\delta_{s\downarrow}^{Cr@C_{60}}$, with decreasing energy. Indeed, the decrease in $\delta_{s\downarrow}^{Cr}$ occurs at $\epsilon \approx 0.3$ eV [23], whereas the corresponding decrease in $\delta_{s\downarrow}^{Cr@C_{60}}$ is seen to occur at $\epsilon \approx 1.7$ eV. We associate this difference with the C_{60}-spin-charging effect due to which the C_{60} cage in $Cr@C_{60}$ becomes primarily spin-up charged. As for the free-Cr phase shift $\delta_{s\uparrow}^{Cr}$, it, in contrast to $\delta_{s\downarrow}^{Cr}$, "enjoys" its monotonic rise towards $\delta_{s\uparrow}^{Cr}(0) = 4\pi$ [23]. This is due to the presence of the $4s\uparrow$ subshell in Cr. Then, adding $\delta_{s\downarrow}^{Cr}$ and $\delta_{s}^{C_{60}}$ together, we obtain a monotonic increase of $\delta_{s\uparrow}^{Cr@C_{60}}$ to $(4+1)\pi$ at $\epsilon = 0$, as was found in the direct calculation of $\delta_{s\uparrow}^{Cr@C_{60}}$ depicted in Fig. 7. In the same manner should behave the phase shifts $\delta_{s\uparrow}^{Mn@C_{60}}$ and $\delta_{s\downarrow}^{Mn@C_{60}}$. Indeed, in free Mn, there are both the $4s\uparrow$ and $4s\downarrow$ subshell. Therefore, spin-up and spin-down incident s electrons experience about equal exchange interaction with the $4s$ electrons of Mn which is also about the same as exchange interaction between an incident $s\uparrow$ electron and the $4s\uparrow$ electron in the electron-Cr collision. Therefore, $\delta_{s\uparrow}^{Cr}$, $\delta_{s\uparrow}^{Mn}$, and $\delta_{s\downarrow}^{Mn}$ behave identically, all rising monotonically towards 4π at $\epsilon = 0$, and so are $\delta_{s\uparrow}^{Cr@C_{60}}$, $\delta_{s\uparrow}^{Mn@C_{60}}$, and $\delta_{s\downarrow}^{Mn@C_{60}}$ as well.

Third, note how differently the $d\downarrow$-phase shift $\delta_{d\downarrow}^{Cr@C_{60}}$ behaves compared to the $d\uparrow$-phase shift $\delta_{d\uparrow}^{Cr@C_{60}}$. The same differences are characteristic between the $\delta_{d\downarrow}^{Mn@C_{60}}$ and $\delta_{d\uparrow}^{Mn@C_{60}}$ phase shifts as well. The noted differences can be explained exactly in the same manner as the just discussed differences between the spin-up and spin-down s-phase shifts in the electron-$Cr@C_{60}$ collision, or the differences between the spin-up and spin-down f-phase shifts in the electron-$Eu@C_{60}$ collision discussed earlier in the paper.

Fourth, note how the phase shift $\delta_{d\downarrow}^{Cr@C_{60}}$ upon electron-$Cr@C_{60}$ collision differs from that $\delta_{d\downarrow}^{Mn@C_{60}}$ upon electron-$Mn@C_{60}$ collision. Namely, the low-energy minimum in $\delta_{d\downarrow}^{Mn@C_{60}}$ is narrower and emerges at lower energies than the minimum in $\delta_{d\downarrow}^{Cr@C_{60}}$. This, however, can easily be tracked back to the differences between the corresponding free-Cr and free-Mn phase shifts depicted in Fig. 7 as well: the free-Mn phase shift $\delta_{d\downarrow}^{Mn}$ starts rapidly decreasing at a lower

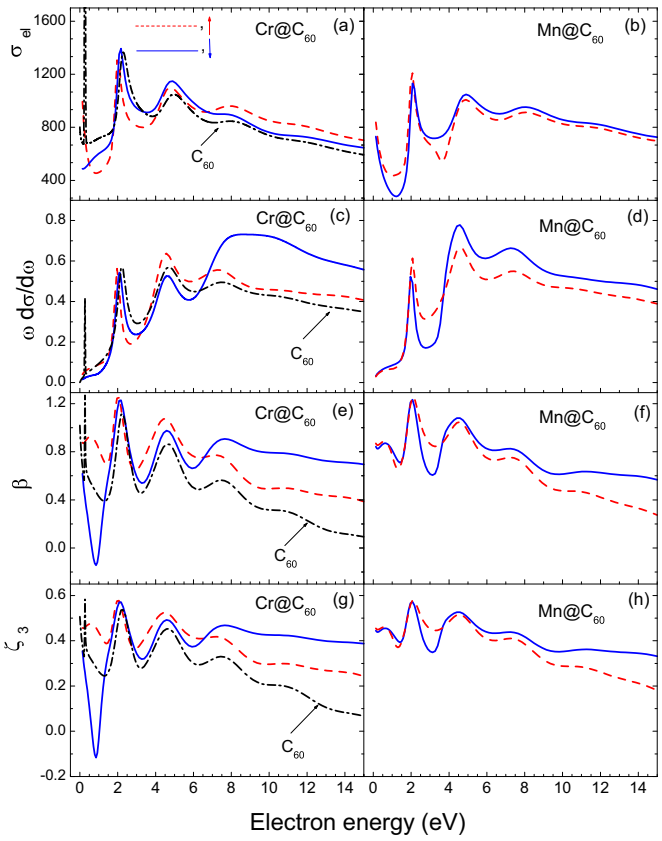

FIG. 8. (Color online) Calculated SPHF spin-down (solid lines) and spin-up (dashed lines) total electron elastic-scattering cross section $\sigma_{\mathrm{el}\uparrow(\downarrow)}$ (in units of a_0^2), low-frequency bremsstrahlung cross sections $\omega d\sigma_{\uparrow(\downarrow)}/d\omega$ (in units of kb), bremsstrahlung angular-asymmetry parameter $\beta_{\uparrow(\downarrow)}$, and Stokes polarization parameter $\zeta_3\uparrow(\downarrow)|_{\theta=90^\circ}$ of low-frequency bremsstrahlung off $Cr@C_{60}$ (left column) and $Mn@C_{60}$ (right column), as marked.

energy and at a greater rate than $\delta_{d\downarrow}^{\mathrm{Cr}}$. Then, employing the independent-scattering approximation, it becomes clear why the low-energy minimum in $\delta_{d\downarrow}^{\mathrm{Mn@C_{60}}}$ is narrower and emerges at lower energies than the minimum in $\delta_{d\downarrow}^{\mathrm{Cr@C_{60}}}$.

Finally, the total electron elastic-scattering cross sections $\sigma_{\mathrm{el}\uparrow(\downarrow)}$ for incident spin-up and spin-down electrons, bremsstrahlung cross sections $\omega d\sigma_{\uparrow(\downarrow)}/d\omega$, angular-asymmetry parameter $\beta_{\uparrow(\downarrow)}$, and Stokes polarization parameter $\zeta_3\uparrow(\downarrow)|_{\theta=90^\circ}$ of low-frequency bremsstrahlung off $Cr@C_{60}$ and $Mn@C_{60}$ are depicted in Fig. 8 along with those for electron collision with empty C_{60}, for comparison.

Similarly to electron collision with empty C_{60}, the resonance maxima in the calculated elastic-scattering and bremsstrahlung quantities are due to the resonances in incident electronic waves with $\ell = 4,5$, and 6, respectively. Calculations showed that the extremely narrow $f\uparrow$ and $f\downarrow$ quasiresonances emerge at the electron energy $\epsilon \approx 0.05$ eV. The latter, however, is outside of the energy range scale of the figure for which reason they are not seen in the figure.

Next, one can see that differences between the spin-up and spin-down calculated quantities are generally stronger in the case of $Cr@C_{60}$ than in the case of $Mn@C_{60}$. This is attributed to the following. First, Cr is a higher-spin atom than Mn, so that spin-dependence of scattering reactions brought about by exchange interaction is stronger in the electron-$Cr@C_{60}$ than in the electron-$Mn@C_{60}$ collision. Second, the C_{60} cage is spin-up charged in $Cr@C_{60}$ but primarily spin-down charged in $Mn@C_{60}$; this induces, implicitly, additional features in exchange interaction of incident electrons with $Cr@C_{60}$ compared to $Mn@C_{60}$.

Furthermore, one encounters once a again the situation where electron elastic scattering off "stuffed" C_{60} is noticeably weaker than off empty C_{60}. In addition, one sees the repetition of the situation met in the $Eu@C_{60}$ case. Namely, the difference between collision of spin-up and spin-down electrons with the considered systems is stronger in calculated bremsstrahlung parameters than in electron elastic-scattering cross sections. The difference is particularly strong in the electron-$Cr@C_{60}$ bremsstrahlung cross section $\omega d\sigma_{\uparrow(\downarrow)}/d\omega$ above about 6 eV. In the corresponding angular asymmetry $\beta_{\uparrow(\downarrow)}$ and Stokes polarization parameter $\zeta_3\uparrow(\downarrow)|_{\theta=90^\circ}$, the above discussed difference happens at around approximately 0.8 eV. There, for example, the spin-down Stokes polarization parameter $\zeta_3^{\mathrm{Cr@C_{60}}}\downarrow$ changes its sign twice in the narrow energy region around 0.8 eV, whereas the spin-up parameter remains always positive.

IV. CONCLUSION

The present work has provided detailed insight into possible features of low-energy electron elastic scattering and low-frequency bremsstrahlung upon electron collisions with $A@C_{60}$ fullerenes gained in the framework of the simple and yet reasonable model static-exchange approximation. This was achieved by studying the dependence of these processes on the individuality of encapsulated atoms A and spin polarization of incident electrons. Results of the work identify, at the given level of approximation, the most interesting and/or useful future measurements or more rigorous calculations to perform. The present study also provides researchers with background information which is useful for future studies aimed at elucidating of the significance of dynamical polarization, correlation effects, molecular-structure effects, etc., in these processes. These processes, particularly polarization of $A@C_{60}$ by incident electrons, will make the $A@C_{60}$ potential more attractive, so that predicated resonances and other features may appear at different energies, or disappear at all, and some actual bound states may be converted to resonances. A thorough discussion of possible consequences of all this is provided in Ref. [7] for the case of electron elastic scattering off empty C_{60}. Obviously, the presence of the atom encapsulated inside C_{60}, which will be dynamically polarized dependently or independently of the polarization of the cage itself, and also interacting with the cage in certain ways, will induce additional modifications in the electron-$A@C_{60}$ collision. Such effects, however, are subject to an independent study, some aspects of which we are currently pursuing.

ACKNOWLEDGMENT

This work was supported by NSF Grant No. PHY-1305085.

[1] V. K. Dolmatov, M. B. Cooper, and M. E. Hunter, Electron elastic scattering off endohedral fullerenes A@C_{60}: The initial insight, J. Phys. B **47**, 115002 (2014).

[2] V. K. Dolmatov, J.-P. Connerade, A. S. Baltenkov, and S. T. Manson, Structure and photoionization of confined atoms, Radiat. Phys. Chem. **70**, 417 (2004).

[3] M. J. Puska and R. M. Nieminen, Photoabsorption of atoms inside C_{60}, Phys. Rev. A **47**, 1181 (1993).

[4] M. Ya. Amusia, V. K. Dolmatov, and L. V. Chernysheva, Confinement and correlation effects in the Xe@C_{60} generalized oscillator strengths, Phys. Rev. A **84**, 063201 (2011).

[5] T.-G. Lee, J. A. Ludlow, and M. S. Pindzola, Sensitivity of cross sections to the diffuseness of the confining potential in time-dependent close-coupling calculations of the double photoionization of He@C_{60}, Phys. Rev. A **87**, 015401 (2013).

[6] P. C. Deshmukh, A. Mandal, S. Saha, A. S. Kheifets, V. K. Dolmatov, and S. T. Manson, Attosecond time delay in the photoionization of endohedral atoms A@C_{60}: A probe of confinement resonances, Phys. Rev. A **89**, 053424 (2014).

[7] C. Winstead and V. McKoy, Elastic electron scattering by fullerene, C_{60}, Phys. Rev. A **73**, 012711 (2006).

[8] Robert R. Johnson, Free-free transitions: A survey of theoretical results, J. Quant. Spectrosc. Radiat. Transfer **7**, 815 (1967).

[9] M. Ya. Amusia and L. V. Chernysheva, *Computation of Atomic Processes: A Handbook for the ATOM Programs* (IOP, Bristol, 1997).

[10] V. Astapenko, *Polarization Bremsstrahlung on Atoms, Plasmas, Nanostructures, and Solids*, Springer Series on Atomic, Optical, and Plasma Physics, Vol. 72 (Springer-Verlag, Berlin, 2013).

[11] A. V. Korol and A. V. Solov'yov, *Polarization Bremsstrahlung*, Springer Series on Atomic, Optical, and Plasma Physics, Vol. 80 (Springer-Verlag, Berlin, 2014).

[12] W. Jaskólski, Confined many-electron systems, Phys. Rep. **271**, 1 (1996).

[13] A. L. Buchachenko, Compressed atoms, J. Phys. Chem. B **105**, 5839 (2001).

[14] *Theory of Confined Quantum Systems, Part 1*, edited by J. R. Sabin, E. Brändas, and C. A. Cruz, Advances in Quantum Chemistry, Vol. 57 (Academic Press, New York, 2009).

[15] *Theory of Confined Quantum Sytems, Part 2*, edited by J. R. Sabin, E. Brändas, and C. A. Cruz, Advances in Quantum Chemistry, Vol. 58 (Academic Press, New York, 2009).

[16] *Electronic Structure of Quantum Confined Atoms and Molecules*, edited by K. D. Sen (Springer International Publishing, Switzerland, 2014).

[17] M. Ya. Amusia, A. S. Baltenkov, and B. G. Krakov, Photodetachment of negative C_{60}^- ions, Phys. Lett. A **243**, 99 (1998).

[18] L. D. Landau and E. M. Lifshitz, *Quantum Mechanics: Nonrelativistic Theory* (Butterworth-Heinemann, Boston, 2002).

[19] I. I. Sobelman, *Introduction to the Theory of Atomic Spectra* (Pergamon Press, Oxford, 1972).

[20] M. Ya. Amus'ya and A. S. Baltenkov, Electron drag in inverse bremsstrahlung of light, Sov. Phys. JETP **42**, 279 (1975).

[21] J. C. Slater *The Self-Consistent Field for Molecules and Solids* (McGraw-Hill, New York, 1974).

[22] V. K. Dolmatov, M. Ya. Amusia, and L. V. Chernysheva, Electron elastic scattering off a semifilled shell atom: The Mn atom, Phys. Rev. A **88**, 042706 (2013).

[23] V. K. Dolmatov, M. Ya. Amusia, and L. V. Chernysheva, Electron elastic scattering off a spin-polarized Cr atom, Phys. Rev. A **90**, 032717 (2014).

[24] E. Yu. Remeta and V. I. Kelemen, Potential electron elastic scattering by atoms in the spin-polarized approach, J. Phys. B **43**, 045202 (2010).

[25] J.-P. Connerade and V. K. Dolmatov, "C_{60} spin-charging" with an eye on a quantum computer, J. Phys. B **48**, 015007 (2015).

[26] W. Harneit, Fullerene-based electron-spin quantum computer, Phys. Rev. A **65**, 032322 (2002).

[27] R. G. Newton, *Scattering Theory of Waves and Particles* (McGraw-Hill, New York, 1969).

[28] N. F. Mott and H. S. W. Messey, *The Theory of Atomic Collisions* (Clarendon Press, Oxford, 1965).

[29] M. Ya. Amusia (private communication).